AN ASYMPTOTIC STUDY OF OXYGEN TRANSPORT FROM MULTIPLE CAPILLARIES TO SKELETAL MUSCLE TISSUE

MICHÈLE S. TITCOMBE AND MICHAEL J. WARD[1]

Abstract

A mathematical model of the transport of oxygen from capillaries to skeletal muscle tissue is a diffusion problem in a two-dimensional, bounded domain with Neumann and mixed boundary conditions. We consider N capillaries of small but arbitrary cross-sectional shape and demonstrate, for $N > 1$, that this is a singular perturbation problem that involves an infinite expansion of logarithmic terms of the small parameter ε, which characterizes the size of the capillary cross-sections. For $\varepsilon \ll 1$, we use a hybrid asymptotic-numerical method to calculate the steady-state oxygen partial pressure in the tissue correct to within all logarithmic terms. Our results from this hybrid method illustrate the effect of tissue heterogeneities such as mitochondria, variable permeability of the capillary walls and the facilitation of oxygen transport by the presence of myoglobin. The results from the hybrid method compare well with full numerical solutions.

1 Introduction

The analytical study of tissue oxygenation from capillaries has been the focus of considerable research since the original work of Krogh [10] in 1919. In the oxygen distribution process of the micro-circulation, oxygen binds to its carrier, haemoglobin, in red blood cells, which transports it through the arterioles, branching to the capillary networks, to the collecting venules. In the capillaries, the oxygen is released from its carrier and diffuses into the surrounding tissue. The reviews of Popel [14] and Fletcher [4] and references therein provide substantial information on the approaches and advancements of the theoretical research in this area.

In this paper, we study an oxygen transport problem in a two-dimensional domain representing a transverse section of skeletal muscle tissue that receives oxygen from an array of capillaries of small but arbitrary cross-sectional shape (see Fig. 1). Following the approach of many authors (e.g. [7], [14]), we model the transport of oxygen from capillaries to tissue by a passive diffusive process. Assuming Fick's law, $\mathbf{J} = -\mathcal{D}\nabla c$, relating the oxygen flux $\mathbf{J}$ to the gradient of oxygen concentration c, and Henry's law, $c = \alpha p$, and that there is a balance of mass in the tissue, the oxygen partial pressure p satisfies

$$\alpha \frac{\partial p}{\partial t} = \nabla \cdot [\alpha \mathcal{D} \nabla p] - \mathcal{M}\,. \tag{1.1}$$

Here, α is the oxygen solubility coefficient, $\mathcal{D}$ is the oxygen diffusion coefficient and $\mathcal{M}$ is the oxygen consumption rate in the tissue. Also, the oxygen partial pressure p satisfies

[1]Department of Mathematics, University of British Columbia, Vancouver, B. C. Canada, V6T 1Z2. This work was supported by NSERC grant 81541.

appropriate conditions at the capillary walls and on the outer tissue boundary. We will solve the steady-state problem corresponding to (1.1) asymptotically in the limit of small capillary cross-sectional radii in a two-dimensional multiply-connected domain that represents the region occupied by the skeletal muscle tissue.

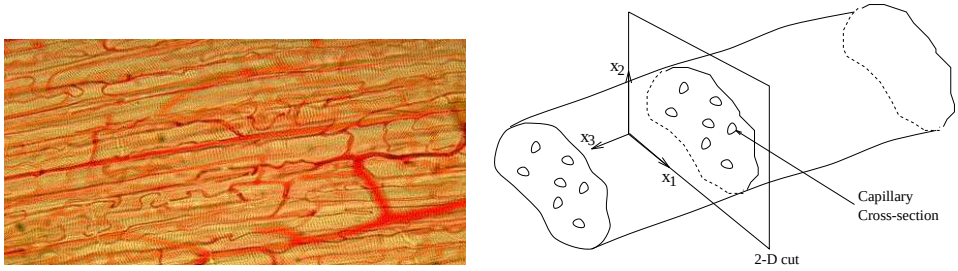

(a) *Actual skeletal muscle tissue* (b) *Mathematical idealization*

Figure 1: *Capillary blood supply in skeletal muscle tissue.*

This model is an extension of the well-known Krogh cylinder model [10] which consists of one capillary of circular cross-section concentric with a circular cross-section of muscle tissue (see Fig. 2). In our extension, we allow for multiple capillaries of arbitrary location, of arbitrary cross-sectional shape, and for the tissue domain to be arbitrary. We also include the effects of tissue heterogeneities, such as oxygen-consuming mitochondria, by choosing the source term $\mathcal{M}$ appropriately, and we allow for the enhancement or facilitation of oxygen transport to the tissue by myoglobin, an iron-protein compound that can reversibly bind up to one oxygen molecule. A comprehensive review of the Krogh cylinder model, and its extensions is in Hoofd [7].

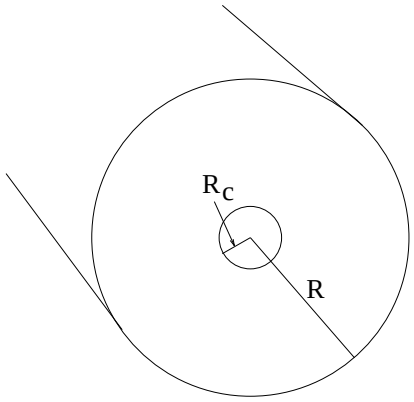

Figure 2: *The Krogh cylinder.*

Most previous attempts to study the oxygenation of muscle tissue analytically have assumed that the capillaries can be represented as point sources for (1.1) (i.e [7], [1], [8], [13]). However, by studying the steady-state diffusion problem systematically using the method of matched asymptotic expansions, we show that this type of rough simplification represents only the leading term in an infinite asymptotic expansion of the oxygen partial pressure in powers of $-1/\log\varepsilon$, where ε is a measure of the capillary cross-section. From a physiological viewpoint, this type of point-source approximation largely ignores the effect of the shape of

the capillary cross-section and the effect of the interaction between the capillaries. When many capillaries are present, the effect of the capillary interaction should be significant. From a mathematical viewpoint, when infinite logarithmic expansions converge they do so very slowly for finite ε, and hence many terms in the asymptotic expansion are necessary to retain sufficient precision in the approximation. Here, by sufficient precision, we refer only to the accurate calculation of a few significant digits in the solution, and not to an unwarranted precision unjustified by the uncertainties in the model. In contrast, the leading term in the logarithmic expansion, represented by the point-source solution, may be quantitatively very inaccurate. Other problems of this type where convergent infinite logarithmic expansions occur and need to be treated accurately are in low Peclet number heat transfer [19], in low Reynolds number flow problems [11], and for eigenvalue problems in multiply-connected two-dimensional domains [20].

From a mathematical perspective, the main goal of this paper is to extend the method of [20] to develop and implement a simple hybrid asymptotic-numerical method to sum the infinite logarithmic expansion for the oxygen partial pressure in the limit of small capillary radii. We present the main result and algorithm in the Proposition of §4. This method allows us to calculate the oxygen partial pressure easily and accurately for arbitrary capillary locations, for arbitrary capillary cross-sectional shapes, and it allows for certain tissue heterogeneities. The numerical analysis involved in calculating the hybrid solution is routine, as it does not require the numerical solution of a stiff problem with boundary layers. From a physiological perspective, in §5, we demonstrate the asymptotic results with some specific examples that illustrate important physiological effects such as capillary interaction; the effect of various cross-sectional shapes of the capillaries; the effect of the locations of the capillaries; variable permeability of the capillary wall; tissue heterogeneities and myoglobin facilitation. A key advantage of our hybrid method is that it allows for a significant reduction in the complexity of this rather large parameter space as compared to using a computationally intensive direct numerical approach on the full problem by the finite element method. As we show in the computing time comparisons in Table 3 of §5, the hybrid method is much faster than a direct numerical approach. The accuracy and simplicity of the hybrid method combined with the significant reduction of the parameter space should benefit physiologists who wish to explore the large parameter space associated with (1.1).

Finally, we remark that our careful study of (1.1) provides only the first step in studying a more biologically realistic model where other effects inside each capillary, such as convective blood flow and pressure variations along the length of the capillary, are included. However, since our asymptotic study of (1.1) shows how to decouple the problem of oxygenation of tissue away from the capillaries asymptotically from any detailed processes occurring near each capillary, our basic framework may be extended to treat a model asymptotically where detailed transport mechanisms occur within each capillary.

In §2, we formulate a dimensionless oxygen transport model, its boundary conditions, and we discuss various assumptions of our model. In §3, we illustrate the asymptotic structure of the solution in the limit of small capillary radius when the capillaries have a circular cross-section with a common radius ε. In §4, we present the hybrid asymptotic-numerical method to solve for the oxygen partial pressure for thin capillaries of arbitrary cross-sectional shape. In §5, we illustrate the hybrid method by varying certain physiological parameters in computing the solution. Finally, in §6, we briefly discuss a few extensions of the methodology.

2 Oxygen Transport Model and Assumptions

We begin by introducing the steady-state, dimensionless model of oxygenation of a two-dimensional skeletal muscle tissue domain D from N small capillaries D_i^ε of arbitrary cross-sectional shape (see Fig. 3). We solve the mathematical model for the steady-state dimensionless oxygen partial pressure $p(\mathbf{x};\varepsilon)$ satisfying

$$\nabla \cdot [\mathcal{P}\nabla p] = \mathcal{M}, \qquad \mathbf{x} \in D \setminus \bigcup_{i=1}^{N} D_i^\varepsilon, \tag{2.1a}$$

$$\varepsilon\mathcal{P}\frac{\partial p}{\partial n} + \kappa_i(p - p_{ci}) = 0, \qquad \mathbf{x} \in \partial D_i^\varepsilon,\ i = 1, \ldots, N, \tag{2.1b}$$

$$\frac{\partial p}{\partial n} = 0, \qquad \mathbf{x} \in \partial D. \tag{2.1c}$$

Here, $\mathbf{x} = (x_1, x_2)$ and we rendered the quantities in our model dimensionless with respect to a characteristic length scale of the tissue domain, L^*; a characteristic oxygen partial pressure, p^*; and the transverse diffusivity, $\mathcal{P}_\mathbf{x}^*$. With these scalings, the dimensionless oxygen consumption rate is $\mathcal{M} = L^{*2}\mathcal{M}^*/(\mathcal{P}_\mathbf{x}^* p^*)$. The small, dimensionless parameter, ε, represents the order of magnitude of the capillary cross-sections, which we assume to be independent of the axial direction. To justify the two-dimensional approximation partially, we observe from Fig. 4 that the arrangement of the capillaries is, for the most part, parallel to the surrounding muscle fibres.

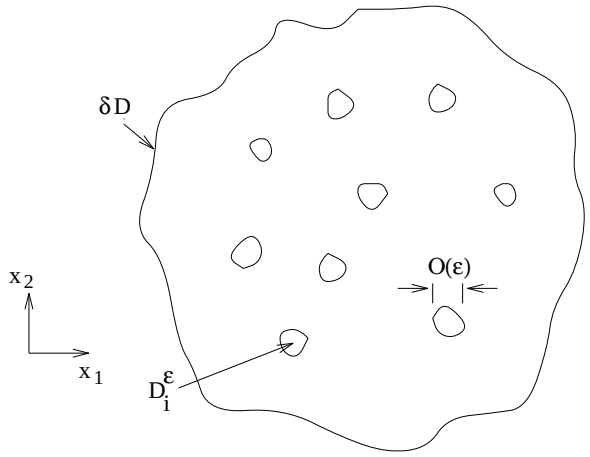

Figure 3: *Our general model for $i = 1, \ldots, N$ capillaries of arbitrary shape of magnitude of order ε in a tissue domain D with boundary ∂D.*

The boundary condition (2.1b) models the capillary wall as a finitely-permeable membrane, where κ_i is the permeability coefficient of the ith capillary and p_{ci} is the oxygen partial pressure within the ith capillary (assumed constant). The limit $\kappa_i \to \infty$ represents an infinitely-permeable capillary wall for the ith capillary, or equivalently that the oxygen partial pressure p at the boundary of the ith capillary is equal to the constant capillary pressure, p_{ci}, of that capillary. In contrast, the limit $\kappa_i \to 0$ leads to the unphysical case of a perfectly-insulating capillary. In (2.1b) and (2.1c), $\partial/\partial n$ is the directional derivative along the outward normal to the tissue domain.

We incorporate skeletal muscle tissue heterogeneities, such as oxygen-consuming mitochondria, through the oxygen diffusivity $\mathcal{P}$ in (2.1a) and (2.1b) and the consumption rate

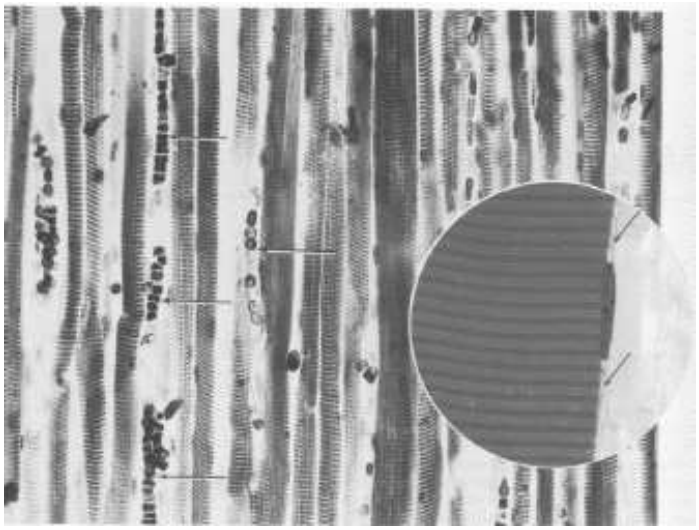

Figure 4: *Photomicrograph of a longitudinally sectioned skeletal muscle, displaying the parallel arrangement of the capillaries (arrows) between the fibres (reproduced from "Histology: A Text and Atlas" [16]).*

of oxygen $\mathcal{M}$ in (2.1a) in the tissue. In homogeneous tissue models, both $\mathcal{P}$ and $\mathcal{M}$ are assumed constant, which one can interpret as having regularly distributed mitochondria throughout the tissue. We assume that the rate of irreversible oxygen consumption in tissue is independent of p, i.e. $\mathcal{M} = \mathcal{M}_0(\mathbf{x})$, which is known as zero-order kinetics. In §6, we consider the effect of other types of kinetics where M depends on p.

We represent the localized consumption of oxygen by m mitochondria with a spatially-dependent $\mathcal{M}$ of the form

$$\mathcal{M} = \mathcal{M}_0 + \sum_{i=1}^{m} \mathcal{M}_i \exp\left(-\frac{|\mathbf{x} - \boldsymbol{\zeta}_i|^2}{\sigma_i^2}\right). \tag{2.2}$$

Here, we model each mitochondrion by a Gaussian distribution superimposed on a constant background consumption rate $\mathcal{M}_0$. In this way, there is freedom for varying the form of the heterogeneous tissue through the parameters, which are: the location, $\boldsymbol{\zeta}_i$; the amplitude, $\mathcal{M}_i$ (where $\mathcal{M}_i > \mathcal{M}_0$); and the variance, σ_i (σ_i reasonably small), of the ith mitochondrion for $i = 1, \ldots, m$.

The oxygen diffusivity $\mathcal{P}$ within the skeletal muscle tissue can also vary with location, such as near oxygen-consuming mitochondria. Certain theoretical models consider that the tissue is a two-phase medium (eg. [2] [18]), having a constant specified diffusivity within each phase. We incorporate this approach in defining $\mathcal{P}(\mathbf{x})$ to have a Gaussian distribution as we suggested for the mitochondria, with corresponding $\mathcal{P}_0$ and $\mathcal{P}_i$, for $i = 1, \ldots, m$.

The fact that myoglobin is able to bind reversibly to one oxygen molecule can enhance, or facilitate, the diffusion of oxygen into the tissue. To incorporate myoglobin facilitation into our model, we follow Fletcher [5] and define the myoglobin-facilitated pressure p^* as

$$p^* = p + p_F[s(p_c) - s(p^*)]. \tag{2.3}$$

Here, p_c is an average of the capillary oxygen partial pressures, and p_F is the facilitation pressure, which is constant for constant diffusivity $\mathcal{P}$ and is zero if no myoglobin is present

in the tissue. When oxygen and myoglobin are in equilibrium, the myoglobin saturation $s(p)$ has the form

$$s(p) = \frac{p}{p_{0.5} + p}, \tag{2.4}$$

where $p_{0.5}$ is the myoglobin half-saturation pressure. To obtain the myoglobin-facilitated oxygen partial pressure, $p^*(\mathbf{x};\varepsilon)$, we solve for p in the absence of myoglobin from (2.1) and substitute into (2.3) to calculate p^*.

3 Asymptotic Structure of the Solution

In this section, we use the method of matched asymptotic expansions to demonstrate that the asymptotic solution to (2.1) for $N > 1$ capillaries involves an infinite expansion of reciprocal logarithms in terms of the small parameter, ε, representing the size of the capillary cross-sections. For ease of illustrating this asymptotic solution structure, we consider the special case of N capillaries with equal, circular cross-sections of radius ε. In the next section, we will apply a hybrid asymptotic-numerical method, which exploits this asymptotic solution structure, to (2.1) with arbitrarily-shaped capillary cross-sections to determine an asymptotic solution correct to within all logarithmic terms.

In a simple version of (2.1) using the Krogh cylinder geometry (Fig. 2 with $R_c = \varepsilon$ and $R = 1$), where $N = 1$ and $\mathcal{P} = 1$, the exact solution for the oxygen partial pressure, p_E, is purely radial and is

$$p_E(r) = p_c + \frac{\mathcal{M}}{2}\left[\frac{r^2 - \varepsilon^2}{2} + \frac{\varepsilon^2 - 1}{\kappa} + \log\left(\frac{\varepsilon}{r}\right)\right]. \tag{3.1}$$

This is an extension of the classic Krogh-Erlang solution [10] that includes variable capillary permeability through the parameter κ. As $\varepsilon \to 0$, the dominant term in (3.1) is $O(\log\varepsilon)$. This suggests that in the global (outer) region away from the capillaries, where $N > 1$, we expand the solution to (2.1) in the form

$$p(\mathbf{x};\varepsilon) = \left(-\frac{1}{\log\varepsilon}\right)^{-1} p^{(0)}(\mathbf{x}) + p^{(1)}(\mathbf{x}) + \sum_{j=2}^{\infty}\left(-\frac{1}{\log\varepsilon}\right)^{j-1} p^{(j)}(\mathbf{x}) + \cdots. \tag{3.2}$$

This global expansion is valid for $|\mathbf{x} - \boldsymbol{\xi}_i| = O(1)$, for $i = 1, \ldots, N$, where $\boldsymbol{\xi}_i$ is the centroid of the ith capillary cross-section. Following (3.18), we show that the effect of capillary interaction for $N > 1$ leads to the infinite sum of logarithmic terms in (3.2), which is in contrast to the case for $N = 1$ in (3.1), where the logarithmic expansion terminates at the first term. For the corresponding ith local (inner) region, which is valid near the ith capillary located at $\mathbf{x} = \boldsymbol{\xi}_i$, we define the local variables $\mathbf{y}_i = \varepsilon^{-1}(\mathbf{x} - \boldsymbol{\xi}_i)$ and $q_i(\mathbf{y}_i;\varepsilon) = p(\varepsilon\mathbf{y}_i + \boldsymbol{\xi}_i;\varepsilon)$. In the ith local region, we expand the solution as

$$q_i(\mathbf{y}_i;\varepsilon) = p_{ci} + q_i^{(1)}(\mathbf{y}_i) + \left(-\frac{1}{\log\varepsilon}\right) q_i^{(2)}(\mathbf{y}_i) + \cdots. \tag{3.3}$$

Here, p_{ci} is a specified constant that represents the oxygen partial pressure within the ith capillary, for $i = 1, \ldots, N$. Substituting the local variables into (2.1a)–(2.1b) and using $\mathcal{P}(\varepsilon\mathbf{y}_i + \boldsymbol{\xi}_i) \approx \mathcal{P}(\boldsymbol{\xi}_i) + O(\varepsilon)$, we find that, to leading order in ε, $q_i(\mathbf{y}_i;\varepsilon)$ satisfies

$$\Delta_y q_i = 0, \qquad \mathbf{y}_i \notin D_i^0, \tag{3.4a}$$

$$\mathcal{P}(\boldsymbol{\xi}_i)\frac{\partial q_i}{\partial n} + \kappa_i(q_i - p_{ci}) = 0, \qquad \mathbf{y}_i \in \partial D_i^0. \tag{3.4b}$$

Here, D_i^0 is the scaled ith capillary, such that $D_i^\varepsilon = \varepsilon D_i^0$, and ∂D_i^0 is its boundary. In this section, D_i^ε is a circle of radius ε and hence, D_i^0 is a circle of radius 1. The missing far-field condition in (3.4) comes from a condition that the local solution match with the global solution in some overlap region of validity. To allow for matching to the global region solution, it is necessary for each $q_i(\mathbf{y}_i)$ to grow logarithmically as $|\mathbf{y}_i| \to \infty$, for $i = 1, \ldots, N$.

Substituting (3.3) into (3.4), we find that all the local region problems for $q_i^{(j)}$ are the same. Thus, we can write $q_i^{(j)} = a_i^{(j)} q_i^{(c)}$ for $j \geq 1$, where $a_i^{(j)}$ are unknown constants that we will determine through the matching process. Here, $q_i^{(c)}(\mathbf{y}_i)$ is the canonical local solution satisfying

$$\Delta_y q_i^{(c)} = 0, \qquad \mathbf{y}_i \notin D_i^0, \tag{3.5a}$$

$$\mathcal{P}(\boldsymbol{\xi}_i)\frac{\partial q_i^{(c)}}{\partial n} + \kappa_i q_i^{(c)} = 0, \qquad \mathbf{y}_i \in \partial D_i^0, \tag{3.5b}$$

$$q_i^{(c)} \sim \log|\mathbf{y}_i| + \frac{\mathcal{P}(\boldsymbol{\xi}_i)}{\kappa_i}, \qquad |\mathbf{y}_i| \to \infty. \tag{3.5c}$$

Returning to the global region, we substitute (3.2) into (2.1a) and (2.1c) to obtain the problems for $p^{(j)}(\mathbf{x})$ for $j \geq 0$. The problem to solve for $p^{(0)}(\mathbf{x})$ is

$$\nabla \cdot [\mathcal{P}\nabla p^{(0)}] = 0, \qquad \mathbf{x} \in D \backslash \bigcup_{i=1}^{N} \{\boldsymbol{\xi}_i\}, \tag{3.6a}$$

$$\frac{\partial p^{(0)}}{\partial n} = 0, \qquad \mathbf{x} \in \partial D. \tag{3.6b}$$

As well, we require that $p^{(0)}$ is regular as $\mathbf{x} \to \boldsymbol{\xi}_i$ for $i = 1, \ldots, N$. The solution to this problem is that $p^{(0)}$ is a constant. We will show later in this section how we determine this constant. The remaining global region problems for $p^{(j)}(\mathbf{x})$, $j \geq 1$, are

$$\nabla \cdot [\mathcal{P}\nabla p^{(j)}] = e_{j1}\mathcal{M}(\mathbf{x}), \qquad \mathbf{x} \in D \backslash \bigcup_{i=1}^{N} \{\boldsymbol{\xi}_i\}, \tag{3.7a}$$

$$\frac{\partial p^{(j)}}{\partial n} = 0, \qquad \mathbf{x} \in \partial D. \tag{3.7b}$$

In (3.7a), e_{jk} is the Kronecker delta function defined by: $e_{jk} = 1$ if $j = k$, and $e_{jk} = 0$ otherwise. In addition to satisfying (3.7), $p^{(j)}(\mathbf{x})$ is singular as $\mathbf{x} \to \boldsymbol{\xi}_i$ for $i = 1, \ldots, N$.

In anticipation of matching the local and global region expansions, we write the ith local expansion in (3.3) as $|\mathbf{y}_i| \to \infty$, in terms of global variables, as

$$\begin{aligned} q_i(\mathbf{y}_i;\varepsilon) \sim & p_{ci} + a_i^{(1)}\{\log|\mathbf{x}-\boldsymbol{\xi}_i| - \log\varepsilon + \mathcal{P}(\boldsymbol{\xi}_i)/\kappa_i\} + \\ & \left(-\frac{1}{\log\varepsilon}\right) a_i^{(2)}\{\log|\mathbf{x}-\boldsymbol{\xi}_i| - \log\varepsilon + \mathcal{P}(\boldsymbol{\xi}_i)/\kappa_i\} + \cdots . \end{aligned} \tag{3.8}$$

Here, we have used (3.5c) and the fact that the local solutions are constant multiples of a canonical local solution, i.e. $q_i^{(j)} = a_i^{(j)} q_i^{(c)}$. As well, at this stage, we can see the convenience of the negative sign in the reciprocal logarithmic gauge functions. The constants p_{ci}, $\mathcal{P}(\boldsymbol{\xi}_i)$ and κ_i, for $i = 1, \ldots, N$, are known; and $a_i^{(j)}$ are unknowns to be determined through matching to the global region solution. In the next section, we will show how the hybrid asymptotic-numerical method avoids having to determine each $a_i^{(j)}$ individually.

In the matching procedure, we compare the global expansion in (3.2) as $\mathbf{x} \to \boldsymbol{\xi}_i$, for $i = 1, \ldots, N$, with (3.8). Comparing the $O(\log \varepsilon)$ terms, we see that matching requires

$$a_1^{(1)} = a_2^{(1)} = \ldots = a_N^{(1)} = p^{(0)}. \tag{3.9}$$

As well, the matching procedure provides the structure of the global region solution $p^{(j)}(\mathbf{x})$ for $j \geq 1$, as $\mathbf{x} \to \boldsymbol{\xi}_i$ for $i = 1, \ldots, N$, which is

$$p^{(j)} \sim a_i^{(j)} \left(\log |\mathbf{x} - \boldsymbol{\xi}_i| + \mathcal{P}(\boldsymbol{\xi}_i)/\kappa_i \right) + a_i^{(j+1)} + e_{j1} p_{ci} + \cdots, \qquad \mathbf{x} \to \boldsymbol{\xi}_i, \ i = 1, \ldots, N. \tag{3.10}$$

The solutions $p^{(j)}(\mathbf{x})$, for $j \geq 1$, which satisfy (3.7) and (3.10) are unique up to an additive constant. For each $j \geq 1$, we decompose the solution $p^{(j)}(\mathbf{x})$ to (3.7) and (3.10) in the form

$$p^{(j)}(\mathbf{x}) = 2\pi \sum_{i=1}^{N} a_i^{(j)} \mathcal{P}(\boldsymbol{\xi}_i) G(\mathbf{x}; \boldsymbol{\xi}_i) + e_{j1} p_R^{(1)}(\mathbf{x}) + a_G^{(j)}. \tag{3.11}$$

On the right-hand side of (3.11), the summation term involves a modified Green's function, the next term involves a regular function that only appears in the $j = 1$ solution (due to the form of the right-hand side of (3.7a)) and the final term is an additive constant, $a_G^{(j)}$, to be determined. In Appendix B, we derive a solvability condition for $p^{(j)}(\mathbf{x})$, which is

$$\sum_{i=1}^{N} a_i^{(j)} \mathcal{P}(\boldsymbol{\xi}_i) = \begin{cases} -\dfrac{1}{2\pi} \displaystyle\int_D \mathcal{M}(\mathbf{x})\, d\mathbf{x}, & j = 1, \\ 0, & j \geq 2. \end{cases} \tag{3.12}$$

In (3.11), $G(\mathbf{x}; \boldsymbol{\zeta})$ is the modified Green's function satisfying

$$\nabla \cdot [\mathcal{P} \nabla G] = -\frac{1}{A_D}, \qquad \mathbf{x} \in D \backslash \{\boldsymbol{\zeta}\}, \tag{3.13a}$$

$$\frac{\partial G}{\partial n} = 0, \qquad \mathbf{x} \in \partial D, \tag{3.13b}$$

$$G \sim \frac{1}{2\pi \mathcal{P}(\boldsymbol{\zeta})} \log |\mathbf{x} - \boldsymbol{\zeta}| + R(\boldsymbol{\zeta}), \qquad \mathbf{x} \to \boldsymbol{\zeta}, \tag{3.13c}$$

$$\int_D G(\mathbf{x}; \boldsymbol{\zeta})\, d\mathbf{x} = 0. \tag{3.13d}$$

In (3.13a), A_D is the area of the region D and in (3.13c), $R(\boldsymbol{\zeta})$ is the regular part of the modified Green's function. We determine $R(\boldsymbol{\zeta})$ uniquely from the solution to (3.13). Also in (3.11), $p_R^{(1)}(\mathbf{x})$ is a regular function, as $\mathbf{x} \to \boldsymbol{\xi}_i$, $i = 1, \ldots, N$, that satisfies

$$\nabla \cdot [\mathcal{P} \nabla p_R^{(1)}] = \mathcal{M}(\mathbf{x}) - \frac{1}{A_D} \int_D \mathcal{M}(\mathbf{x})\, d\mathbf{x}, \qquad \mathbf{x} \in D, \tag{3.14a}$$

$$\frac{\partial p_R^{(1)}}{\partial n} = 0, \qquad \mathbf{x} \in \partial D, \tag{3.14b}$$

$$\int_D p_R^{(1)}(\mathbf{x})\, d\mathbf{x} = 0. \tag{3.14c}$$

In the right-hand side of (3.14a), we used (3.12).

Using (3.13c) in (3.11), we obtain a second expression for the structure of $p^{(j)}(\mathbf{x})$ as $\mathbf{x} \to \boldsymbol{\xi}_i$, $i = 1, \ldots, N$, which is

$$p^{(j)} \sim a_i^{(j)} \log|\mathbf{x} - \boldsymbol{\xi}_i| + 2\pi a_i^{(j)} \mathcal{P}(\boldsymbol{\xi}_i) R(\boldsymbol{\xi}_i) + 2\pi \sum_{\substack{k=1 \\ k \neq i}}^{N} a_k^{(j)} \mathcal{P}(\boldsymbol{\xi}_k) G(\boldsymbol{\xi}_i; \boldsymbol{\xi}_k) + e_{j1} p_R^{(1)}(\boldsymbol{\xi}_i) + a_G^{(j)} + o(1). \tag{3.15}$$

Comparing the expression in (3.15) with (3.10), we find that the $\log|\mathbf{x} - \boldsymbol{\xi}_i|$ terms automatically agree. From the remaining terms, we see that

$$2\pi a_i^{(j)} \mathcal{P}(\boldsymbol{\xi}_i) R(\boldsymbol{\xi}_i) + 2\pi \sum_{\substack{k=1 \\ k \neq i}}^{N} a_k^{(j)} \mathcal{P}(\boldsymbol{\xi}_k) G(\boldsymbol{\xi}_i; \boldsymbol{\xi}_k) + e_{j1} p_R^{(1)}(\boldsymbol{\xi}_i) + a_G^{(j)} = a_i^{(j+1)} + e_{j1} p_{ci} + a_i^{(j)} \mathcal{P}(\boldsymbol{\xi}_i)/\kappa_i, \tag{3.16}$$

for $i = 1, \ldots, N$ and $j \geq 1$. These are N equations for the $N + 1$ unknowns: $a_i^{(j+1)}$, for $i = 1, \ldots, N$, and $a_G^{(j)}$ at each level j. The solvability condition in (3.12) provides the last equation for these unknowns. Thus, we solve (3.16) and (3.12) recursively to find $a_i^{(j+1)}$, for $i = 1, \ldots, N$, and $a_G^{(j)}$ for each $j \geq 1$. To determine the constant $p^{(0)}$, and hence the constants $a_i^{(1)}$ for $i = 1, \ldots, N$, which we require to start the recursion, we use (3.12) with $j = 1$ and (3.9) to obtain

$$p^{(0)} = -\frac{\int_D \mathcal{M}(\mathbf{x})\, d\mathbf{x}}{2\pi \sum_{i=1}^{N} \mathcal{P}(\boldsymbol{\xi}_i)} = a_i^{(1)}, \quad i = 1, \ldots, N. \tag{3.17}$$

In summary, with the $a_i^{(1)}$ known, we solve (3.16) and (3.12) recursively to find $a_i^{(j+1)}$, for $i = 1, \ldots, N$, and $a_G^{(j)}$ for each $j \geq 1$.

At this point, it is worth reflecting over the form of the asymptotic solution. For the special case of a single capillary in the tissue domain (i.e. $N = 1$), the solvability condition in (3.12) gives that

$$a_1^{(j)} = 0, \qquad j \geq 2. \tag{3.18}$$

Substituting (3.18) into (3.16) gives that $a_G^{(j)} = 0$ for $j \geq 2$. From the expression for the global solution in (3.11), for this special case of one capillary, we see that $p^{(j)}(\mathbf{x}) = 0$ for $j \geq 2$. When we substitute this information into the global expansion in (3.2), we obtain that the solution for the one-capillary problem has a finite number of terms. However, for $N > 1$, the recursive solution to (3.12) and (3.16) results in non-zero values for $a_i^{(j)}$ and $a_G^{(j)} = 0$ for $j \geq 1$. Thus, using (3.11) in (3.2), the asymptotic solution for the oxygen partial pressure, in a tissue domain containing $N > 1$ capillaries, involves an infinite expansion in terms of reciprocal logarithmic gauge functions.

Hoofd [8] and Clark et al. [1], who consider multiple-capillary models by representing capillaries as point sources, do not sum the infinite logarithmic expansion contained in the solution. As we mentioned in the introduction, the convergence of such a series is very slow

for finite ε and hence, to obtain an accurate solution with an error that is algebraic in ε, it is necessary to sum the expansion.

In the next section, we examine the solution to (2.1) via a hybrid asymptotic-numerical method which exploits the asymptotic solution structure that we outlined above to avoid the daunting task of determining each set of coefficients, $a_i^{(j)}$, at each $j \geq 1$.

4 Solution Using a Hybrid Asymptotic-Numerical Method

We now apply the hybrid asymptotic-numerical method to solving (2.1) with N capillaries of arbitrary cross-sectional shape.

As the first step of the hybrid method, we rewrite the ith local expansion from (3.3) to include a function containing all the logarithmic terms of the solution in the form

$$q_i(\mathbf{y}_i;\varepsilon) = p_{ci} + Q_i^{(0)}(\mathbf{y}_i;\nu_1,\ldots,\nu_N) + \varepsilon Q_i^{(1)}(\mathbf{y}_i;\nu_1,\ldots,\nu_N) + \cdots , \tag{4.1a}$$

where

$$Q_i^{(0)}(\mathbf{y}_i;\nu_1,\ldots,\nu_N) = A_i(\nu_1,\ldots,\nu_N) q_i^{(c)}(\mathbf{y}_i) . \tag{4.1b}$$

Here, ν_i is the reciprocal logarithmic gauge function

$$\nu_i \equiv -\frac{1}{\log(\varepsilon d_i)} . \tag{4.1c}$$

The constants, A_i for $i = 1,\ldots,N$, which incorporate all of the logarithmic terms in the expansion as we outlined in §3, are to be determined. The function $q_i^{(c)}(\mathbf{y}_i)$ is the canonical local solution satisfying (3.5a)–(3.5b) and

$$q_i^{(c)} \sim \log|\mathbf{y}_i| - \log d_i + \cdots , \qquad |\mathbf{y}_i| \to \infty . \tag{4.2}$$

The problem (3.5a)–(3.5b), together with the far-field condition (4.2), uniquely determine the parameter d_i, which is known as the logarithmic capacity. This constant depends on the shape of the scaled capillary cross-section D_i^0, on κ_i, and on $\mathcal{P}(\boldsymbol{\xi}_i)$. For a specific cross-sectional shape of the ith capillary, we must compute numerically the shape-dependent parameter d_i from the solution to (3.5a)–(3.5b) and (4.2). In some cases, such as for a circular or elliptic cross-sectional shape, it is possible to determine d_i analytically (see the Appendix in Titcombe & Ward [19]). For a circular capillary of radius ε, we can solve for $q_i^{(c)}$ exactly to calculate

$$d_i = \exp(-\mathcal{P}(\boldsymbol{\xi}_i)/\kappa_i) . \tag{4.3}$$

For the particular case of $\kappa_i = \infty$, Ransford [15] provides a table of capacities d_i, which we have included in Table 1 for certain typical cross-sectional shapes.

Using $Q_i^{(0)} = A_i q_i^{(c)}$ and (4.2) in (4.1a), we have that the far-field structure of the local region solution, in terms of global region variables, is

$$q_i(\mathbf{y}_i;\varepsilon) \sim p_{ci} + A_i[\log|\mathbf{x}-\boldsymbol{\xi}_i| + \nu_i^{-1}(\varepsilon d_i)] + \cdots , \qquad |\mathbf{y}_i| \to \infty. \tag{4.4}$$

In the global region, we expand the solution as

$$p(\mathbf{x};\varepsilon) = p_G + P^{(0)}(\mathbf{x};\nu_1,\ldots,\nu_N) + \varepsilon P^{(1)}(\mathbf{x};\nu_1,\ldots,\nu_N) + \cdots . \tag{4.5}$$

D_i^0	d_i
circle, radius r	r
ellipse, semi-axes a and b	$\dfrac{a+b}{2}$
equilateral triangle, side h	$\dfrac{\sqrt{3}\,\Gamma\left(\frac{1}{3}\right)^3 h}{8\pi^2} \approx 0.422h$
isosceles right triangle, short side h	$\dfrac{3^{3/4}\Gamma\left(\frac{1}{4}\right)^2 h}{2^{7/2}\pi^{3/2}} \approx 0.476h$
square, side h	$\dfrac{\Gamma\left(\frac{1}{4}\right)^2 h}{4\pi^{3/2}} \approx 0.5902h$

Table 1: *Capacity d_i for cross-sectional shape D_i^0, for $\kappa_i = \infty$ (adapted from Ransford [15]).*

Here, p_G is a global constant that we will determine along with A_i, for $i = 1, \ldots, N$. We will see that $p_G \sim O(\log \varepsilon)$ as $\varepsilon \to 0$. Substituting (4.5) into (2.1a) and (2.1c), and requiring that the global region solution match to the local region solution, we get that $P^{(0)}(\mathbf{x}; \nu_1, \ldots, \nu_N)$ is the unique solution to

$$\nabla \cdot [\mathcal{P} \nabla P^{(0)}] = \mathcal{M}(\mathbf{x}), \qquad \mathbf{x} \in D \setminus \bigcup_{i=1}^{N} \{\boldsymbol{\xi}_i\}, \tag{4.6a}$$

$$\frac{\partial P^{(0)}}{\partial n} = 0, \qquad \mathbf{x} \in \partial D, \tag{4.6b}$$

$$P^{(0)} \sim A_i \log|\mathbf{x} - \boldsymbol{\xi}_i| + A_i \nu_i^{-1} + p_{ci} - p_G, \qquad \mathbf{x} \to \boldsymbol{\xi}_i, \ i = 1, \ldots, N, \tag{4.6c}$$

$$\int_D P^{(0)}(\mathbf{x})\, d\mathbf{x} = 0. \tag{4.6d}$$

There is a solution to (4.6) provided that

$$\sum_{i=1}^{N} A_i \mathcal{P}(\boldsymbol{\xi}_i) = -\frac{1}{2\pi} \int_D \mathcal{M}(\mathbf{x})\, d\mathbf{x}. \tag{4.7}$$

The solvability condition in (4.7) represents a balance of consumption and production of oxygen in the tissue.

We decompose the solution $P^{(0)}(\mathbf{x}; \nu_1, \ldots, \nu_N)$ in the form

$$P^{(0)}(\mathbf{x}; \nu_1, \ldots, \nu_N) = 2\pi \sum_{i=1}^{N} A_i(\nu_1, \ldots, \nu_N) \mathcal{P}(\boldsymbol{\xi}_i) G(\mathbf{x}; \boldsymbol{\xi}_i) + P_R^{(0)}(\mathbf{x}). \tag{4.8}$$

Here, G is the modified Green's function that satisfies (3.13). As well, $P_R^{(0)}(\mathbf{x})$ is a regular function, as $\mathbf{x} \to \boldsymbol{\xi}_i$, for $i = 1, \ldots, N$, that satisfies (3.14).

Using (3.13c) in (4.8), we obtain that the near-field structure of $P^{(0)}$ is

$$P^{(0)} \sim A_i \log|\mathbf{x}-\boldsymbol{\xi}_i| + 2\pi A_i \mathcal{P}(\boldsymbol{\xi}_i) R(\boldsymbol{\xi}_i) + 2\pi \sum_{\substack{k=1 \\ k\neq i}}^{N} A_k \mathcal{P}(\boldsymbol{\xi}_k) G(\boldsymbol{\xi}_i;\boldsymbol{\xi}_k) + P_R^{(0)}(\boldsymbol{\xi}_i), \quad \text{as} \quad \mathbf{x}\to\boldsymbol{\xi}_i,\ i=1,\ldots,N. \tag{4.9}$$

Comparing (4.6c) and (4.9), we see that the $\log|\mathbf{x}-\boldsymbol{\xi}_i|$ terms automatically agree. From the comparison of the remaining terms, we obtain a set of N equations for the A_i and the constant p_G. The final equation relating these unknowns is (4.7). In this way, we obtain our main result:

Proposition (Hybrid Method): *For $\varepsilon \to 0$, the solution to* (2.1)*, asymptotically near the ith capillary, is*

$$p \sim p_{ci} + A_i q_i^{(c)}(\mathbf{y}_i)\,, \qquad \mathbf{y}_i = \varepsilon^{-1}(\mathbf{x}-\boldsymbol{\xi}_i) = O(1)\,. \tag{4.10a}$$

Here $q_i^{(c)}$ satisfies (3.5a)–(3.5b) *with far-field behavior* (4.2)*. In the global region, defined at $O(1)$ distances from the capillaries, we have*

$$p \sim p_G + 2\pi \sum_{i=1}^{N} A_i \mathcal{P}(\boldsymbol{\xi}_i) G(\mathbf{x};\boldsymbol{\xi}_i) + P_R^{(0)}(\mathbf{x})\,. \tag{4.10b}$$

Here p_G and the constants A_i are determined from the solution to the linear system

$$2\pi A_i \mathcal{P}(\boldsymbol{\xi}_i) R(\boldsymbol{\xi}_i) + 2\pi \sum_{\substack{k=1 \\ k\neq i}}^{N} A_k \mathcal{P}(\boldsymbol{\xi}_k) G(\boldsymbol{\xi}_i;\boldsymbol{\xi}_k) + P_R^{(0)}(\boldsymbol{\xi}_i) = A_i \nu_i^{-1} + p_{ci} - p_G \quad i=1,\ldots,N \tag{4.10c}$$

$$\sum_{i=1}^{N} A_i \mathcal{P}(\boldsymbol{\xi}_i) = -\frac{1}{2\pi}\int_D \mathcal{M}(\mathbf{x})\,d\mathbf{x}. \tag{4.10d}$$

In (4.10b)*, G is the modified Green's function satisfying* (3.13)*, and $R(\boldsymbol{\xi})$ is the regular part of G. The function $P_R^{(0)}$ satisfies* (3.14) *with $p_R^{(1)}$ replaced by $P_R^{(0)}$. In* (4.10c)*, ν_i is defined in terms of the shape-parameter d_i by* (4.1c)*.*

In summary, the parameters to specify in the problem are

ε	order of magnitude of the capillary cross-sections
N	number of capillaries
p_{ci}	oxygen partial pressure within the ith capillary
κ_i	permeability coefficient of the ith capillary wall
$\boldsymbol{\xi}_i$	location of the ith capillary
$\mathcal{P}(\mathbf{x})$	diffusivity in the tissue
$\mathcal{M}(\mathbf{x})$	consumption rate of oxygen in the tissue
D	geometry of the tissue domain.

(4.11)

For a given tissue geometry, for which we specify the given number and location of the capillaries in the tissue domain and the diffusivity function $\mathcal{P}$, we use (3.13) once only to compute the modified Green's function $G(\mathbf{x};\boldsymbol{\zeta})$ and its regular part $R(\boldsymbol{\zeta})$. The simple

numerical procedure for this is in Appendix A. Then, after specifying $\mathcal{M}$, we compute the smooth function $P_R^{(0)}$ from (3.14), and evaluate the solution at the capillary locations $\boldsymbol{\xi}_i$. This information, which is then substituted into (4.10c), represents the numerical part of the hybrid method algorithm. Finally, the effect of the cross-sectional shape of the capillary and the permeability of the capillary wall enters only into the determination of the shape-dependent parameters d_i to be used in $\nu_i = -1/\log(\varepsilon d_i)$ in the right-hand side of (4.10c). This is known as Kaplun's equivalence principle [11], which significantly reduces the complexity of the parameter space, since for a change in shape of the capillary cross-section we only need to re-compute one single constant d_i. The numerical solution to the linear system (4.10c)–(4.10d) then determines the strengths, A_i, of the singularities as functions of ε. Finally, the error associated with the result (4.10) should be algebraic in ε.

There are a couple of ways to try to approximate (4.10c)–(4.10d) when $\varepsilon \ll 1$. Firstly, if we let $\varepsilon \to 0$ in this system, we find that, for a non-trivial solution for A_i in (4.10c) to exist, we require p_G to balance with $A_i \nu_i^{-1}$. This means that $p_G \sim O(\log \varepsilon)$ as $\varepsilon \to 0$ since $A_i \sim O(1)$ as $\varepsilon \to 0$. Secondly, if we neglect the off-diagonal terms in (4.10c) that represent capillary interaction, then we obtain an expression for p_G from the diagonal entries

$$(p_G)_{diag} = \frac{1}{N} \sum_{i=1}^{N} \left(p_{ci} + A_i {\nu_i}^{-1} - 2\pi A_i \mathcal{P}(\boldsymbol{\xi}_i) R(\boldsymbol{\xi}_i) - P_R^{(0)}(\boldsymbol{\xi}_i) \right). \tag{4.12}$$

5 Computational Results

We present our results demonstrating the effect of homogeneous versus heterogeneous tissue with respect to oxygen diffusivity and consumption rate, and the effects of capillary interaction, the cross-sectional shape of the capillaries, variable capillary wall permeability, and myoglobin-facilitated oxygen transport. Although we can consider tissue domains and capillaries of arbitrary shape in our model, we choose simple geometries in the examples to highlight certain effects that are unrelated to the tissue geometry. In certain cases, where possible, we compare to the exact solution or a direct numerical solution of (2.1). We have used *Matlab*, in particular the *Partial Differential Equations Toolbox* [12], for the simple numerics of the hybrid method and for the direct numerical computations. Unless otherwise specified, the discrete points in the plots below are the direct numerical results. These examples illustrate the advantages of the hybrid method: a reduced parameter space through the use of Kaplun's equivalence principle [11] and asymptotic accuracy with less restrictive time and storage requirements than a direct numerical solution.

In Table 2, we list ranges of dimensional parameter values for use in our computations that we obtained from a number of references (eg. [9], [14], [3], [1] and [7]). The dimensionless diffusivity $\mathcal{P}$ and dimensionless capillary pressure p_c are measured relative to their dimensional counterparts (indicated with an $*$). In the examples below, we choose values for our dimensionless parameters, such as the dimensionless oxygen consumption rate $\mathcal{M} = L^{*2}\mathcal{M}^*/(p^*\mathcal{P}^*)$, that correspond to typical dimensional quantities.

Example: Homogeneous versus heterogeneous tissue. For the special case of one circular capillary of radius ε that is concentric with a circular tissue domain D of radius 1 with diffusivity $\mathcal{P} = 1$, the exact solution of (2.1) for the oxygen partial pressure in the tissue is (3.1). In Fig. 5, we have plotted the minimum oxygen partial pressure p_{min} versus the capillary radius ε to compare the hybrid method solution with the exact solution, and for certain values of ε, with the direct numerical solution of (2.1). The

Dimensional Parameter		Range of Values	Units
O_2 consumption rate	$\mathcal{M}^*$	$3.3 \times 10^{-5} \rightarrow 3.1 \times 10^{-2}$	mL-O_2/cm^3-s
Tissue diffusivity	$\mathcal{P}^*$	$3.9 \times 10^{-10} \rightarrow 4.8 \times 10^{-10}$	mL-O_2/cm-s-mm Hg
Tissue O_2 partial pressure	p^*	$26 \rightarrow 30$	mm Hg
Tissue domain length scale	L^*	$1.5 \times 10^{-3} \rightarrow 1.8 \times 10^{-2}$	cm

Table 2: *Range of dimensional parameter values.*

(dimensionless) parameter values for this example are: capillary pressure $p_c = 5$, oxygen consumption rate $\mathcal{M} = 0.5$, and capillary permeability coefficient $\kappa = \infty$ (an infinitely-permeable capillary wall). In homogeneous tissue models, the oxygen diffusivity and oxygen consumption rate are constant. Also in Fig. 5, we have included the corresponding $p_{min}(\varepsilon)$

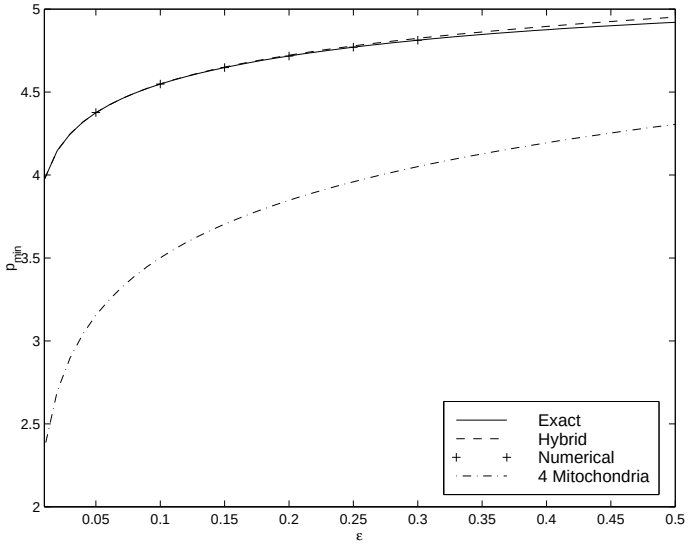

Figure 5: *Minimum oxygen partial pressure p_{min} versus ε, the capillary radius, for a circular tissue domain of radius 1 with one concentric circular capillary. Parameter values: $p_c = 5$, $\mathcal{M} = 0.5$, $\kappa = \infty$, $\mathcal{P} = 1$. Mitochondria parameter values: $\boldsymbol{\zeta}_i = (\pm 0.5, \pm 0.5)$, $\mathcal{M}_0 = 0.5$, $\mathcal{M}_i = 50$, $\mathcal{P}_0 = 1$, $\mathcal{P}_i = 4$, and $\sigma_i = 0.05$, for $i = 1, \ldots, 4$.*

curve for a heterogeneous tissue domain of the same geometry but containing 4 oxygen-consuming mitochondria. We incorporate the mitochondria using the Gaussian distribution form in (2.2) for both $\mathcal{M}(\mathbf{x})$ and $\mathcal{P}(\mathbf{x})$ with parameter values: mitochondria locations $\boldsymbol{\zeta}_i = (\pm 0.5, \pm 0.5)$; variance $\sigma_i = 0.05$; background oxygen consumption rate and diffusivity, $\mathcal{M}_0 = 0.5$ and $\mathcal{P}_0 = 1$ (the same as for the homogeneous tissue); and oxygen consumption rate and diffusivity within the ith mitochondria, $\mathcal{M}_i = 50$ and $\mathcal{P}_i = 4$, for $i = 1, \ldots, 4$. The $p_{min}(\varepsilon)$ curves in Fig. 5 are increasing functions of ε, indicating that the larger the capillary radius, the more oxygen the tissue receives. The heterogeneous tissue $p_{min}(\varepsilon)$ curve lies below that of the homogeneous tissue, given the same background oxygen consumption rate and diffusivity, showing that the presence of the mitochondria lowers the oxygenation in the tissue. The figure also reveals that the hybrid solution agrees well with the exact solution for values of ε up to approximately 0.2. Table 3 contains the time to compute a single point of the homogeneous tissue $p_{min}(\varepsilon)$ curve of Fig. 5. The table shows that the direct

numerical solution took approximately 13 times as long to compute as the hybrid method solution using meshes of comparable refinement.

	$p_{min}(0.05)$	Mesh size (elements)	Time/point (seconds)
Exact	**4.3758**		
Hybrid	4.3760	7680	2.99
Numerical	4.3765	7424	40.49
	4.3759	29696	187.88

Table 3: *CPU time to compute one point, $p_{min}(\varepsilon) = p_{min}(0.05)$, for the homogeneous tissue case of Fig. 5: hybrid method solution versus the direct numerical solution.*

Example: Capillary interaction. We consider $N = 4$ capillaries of circular cross-section with radius ε in a circular tissue domain D of radius 1, and vary the intercapillary spacing to display the effect of capillary interaction on oxygenation of the tissue. Fig. 6(a) shows the locations at $\boldsymbol{\xi}_i^j = (\pm j/4\cos(\pi/4), \pm j/4\sin(\pi/4))$, for $j = 1, 2, 3$ of the $i = 1, \cdots, 4$ capillaries. The parameter values for this example are: diffusivity $\mathcal{P} = 1$ and oxygen consumption rate $\mathcal{M} = 0.3$; capillary permeability coefficients $\kappa_i = \infty$; and intracapillary oxygen partial pressure $p_{ci} = 5$, for $i = 1, \ldots, 4$. With circular cross-sectional shapes of radius ε and with $\kappa_i = \infty$, the shape-dependent parameters are $d_i = 1$, for $i = 1, \cdots, 4$. In the upper plot of Fig. 6(b), we have plotted the minimum oxygen partial pressure p_{min} versus ε, the radius of the capillary cross-sections. For certain values of ε, we have included the results from a direct numerical solution of (2.1). Of the $p_{min}(\varepsilon)$ curves that include interaction effects, the $j = 2$ curve lies uppermost, showing that the tissue receives more oxygen when the capillaries are in this position, than in the other capillary spacings we considered. The hybrid method results compare well with those of the direct numerical computation. Again, the direct numerical solution required significantly more computational effort since it involved redefining the geometry and the grid for each ε and for each set of capillary locations.

There are two ways in which we can test the no interaction limit of the hybrid method solution. One way is to include only the first term on the right-hand side in (4.5), that neglects the capillary interaction term in (4.8). The other way is to neglect the off-diagonal terms, representing interaction, in (4.10c). For the $j = 2$ case, we included the corresponding $p_{min}(\varepsilon)$ curves of p_G, the first term on the right-hand side of (4.5), and of $(p_G)_{diag}$ from (4.12). We see that the $p_{min}(\varepsilon)$ curve corresponding to p_G lies above the other curves, indicating that the global effect of capillary interaction is to lower the oxygenation in the tissue. In their multiple-capillary oxygen transport model, Clark et al. [1] found a reduction in oxygen partial pressure levels in the tissue due to capillary interaction. On the other hand, the $p_{min}(\varepsilon)$ curve corresponding to $(p_G)_{diag}$ lies below all of the other curves, which is what one would expect for the effect of capillary interaction.

For the particular case of four capillaries of radius $\varepsilon = 0.04$, Fig. 7 displays the minimum oxygen partial pressure p_{min} for specific values of r, the radial spacing of the capillaries, that we computed using the hybrid method. Fig. 7 shows that maximum oxygenation occurs when the radial spacing of the capillaries is approximately 0.6 in the tissue domain of radius 1.

Finally, we illustrate the effect of the reduction in the parameter space as a result of

using Kaplun's equivalence principle that we discussed in §4. If, instead of four capillaries of circular cross-sectional area of radius ε, we had four identical ellipses, the results in Fig. 6 still apply provided that we replace the horizontal axis of ε, by εd, where d is in Table 1 for an ellipse with $\kappa = \infty$. Alternatively, if the walls of the four capillaries of circular cross-section are not infinitely permeable, then we would replace the horizontal axis of Fig. 6 by εd, where $d = \exp(-1/\kappa)$ from (4.3) and where κ is the identical permeability coefficient for each capillary.

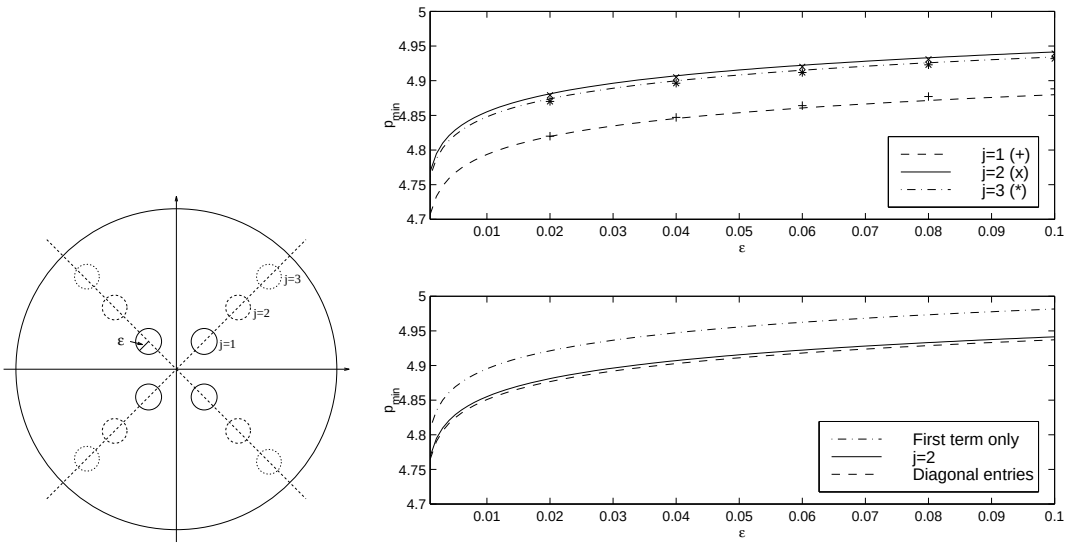

(a) (b)

Figure 6: *(a) Locations of* 4 *circular capillaries at* $(\pm j/4\cos(\pi/4), \pm j/4\sin(\pi/4))$*, for* $j = 1, 2, 3$*, within a circular tissue domain of radius 1. (b) Minimum oxygen partial pressure* p_{min} *versus capillary radius* ε *for the tissue geometry shown in (a). Parameter values:* $p_c = 5$*,* $\mathcal{M} = 0.3$*,* $\kappa = \infty$*,* $\mathcal{P} = 1$*. Upper plot:* $j = 1, 2, 3$ *cases from hybrid solution (curves) and from numerical solution (discrete points). Lower plot: for* $j = 2$ *case, hybrid solution including interaction; and hybrid solution excluding interaction by using only the first term in* (4.5) *and by using the diagonal term approximation in* (4.12)*.*

Example: Capillary cross-sectional shape. We demonstrate the effect of capillary cross-sectional shape for one capillary that is concentric with the rectangular tissue domain, $-2 \le x_1 \le 2$ and $-1.5 \le x_2 \le 1.5$. We assume that $\kappa = \infty$ so that the capillary is infinitely permeable. Then, from Ransford [15], we have d_i for five cross-sectional shapes: (i) circle, (ii) ellipse, (iii) equilateral triangle, (iv) isosceles triangle, and (v) square. With ε as the radius of the circular cross-section, we choose the side length scales for the remaining four shapes so that each of the five boundaries enclose the same area. As in the previous example, we consider homogeneous tissue with diffusivity $\mathcal{P} = 1$ and oxygen consumption rate $\mathcal{M} = 0.5$, and the capillary pressure $p_c = 5$. In Fig. 8, we have plotted the minimum oxygen partial pressure p_{min} versus ε and see that the $p_{min}(\varepsilon)$ curve for the circular cross-sectional shape lies below all the other curves. This illustrates the isoperimetric inequality (see Garabedian [6]) that for various cross-sectional shapes enclosing the same area, the minimum d_i occurs for a circular cross-section. Actual capillary cross-sectional shapes

range from circular to somewhat triangular with rounded edges. The figure suggests that a slight variation from the circular cross-section will increase the oxygenation of the tissue.

Example: Variable capillary wall permeability. To illustrate the effect of variable capillary wall permeability, we consider one circular capillary concentric with an elliptical tissue domain with semi-axes $a = 2$ and $b = 1$. For a circular capillary cross-section, the shape-dependent parameter is $d_i = \exp(-\mathcal{P}(\boldsymbol{\xi}_i)/\kappa_i)$, where $\boldsymbol{\xi}_i$ is the location and κ_i is the capillary wall permeability of the ith capillary. The parameters are: constant diffusivity $\mathcal{P} = 1$, oxygen consumption rate $\mathcal{M} = 0.3$, and capillary pressure $p_c = 5$. Fig. 9 shows the minimum oxygen partial pressure p_{min} as a function of κ for the capillary cross-section of radius $\varepsilon = 0.1$. There is a dramatic variation in minimum pressure for κ up to approximately 10, above which, the capillary wall is essentially infinitely permeable. We note that as $\kappa \to 0$, this solution approaches the physically unreasonable case of a fully insulated capillary wall.

Example: Myoglobin facilitation. Myoglobin is a oxygen-binding protein whose presence in the tissue can enhance or facilitate the transport of oxygen from the capillaries. To demonstrate the effect of myoglobin facilitation, we have plotted in Fig. 10 the oxygen partial pressure $p(x, 0)$ along the positive x-axis radius of the circular tissue domain of radius 1 containing one concentric circular capillary of radius $\varepsilon = 0.05$ in the presence or absence of myoglobin in the tissue. When myoglobin is present, we use (2.3) and (2.4) with facilitation pressure $p_F = 0.5$ and myoglobin half-saturation pressure $p_{0.5} = 1$. For both cases, we use the parameters: oxygen consumption rate $\mathcal{M} = 0.3$, diffusivity $\mathcal{P} = 1$, capillary pressure $p_c = 5$, and capillary permeability coefficient $\kappa = \infty$. The plot indicates that there is more oxygen in the tissue with myoglobin present than without.

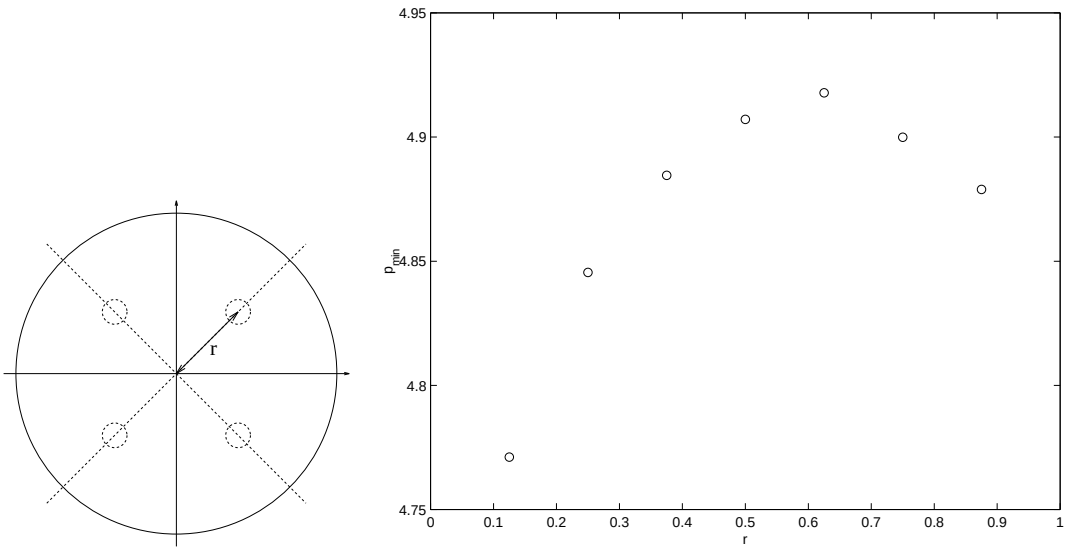

(a) (b)

Figure 7: *(a) Radial spacing r of the 4 capillaries. (b) Minimum oxygen partial pressure p_{min} versus r of 4 circular capillaries of radius $\varepsilon = 0.04$ in a circular tissue domain of radius 1, using the hybrid method. Parameter values: $p_c = 5$, $\mathcal{M} = 0.3$, $\kappa = \infty$, $\mathcal{P} = 1$.*

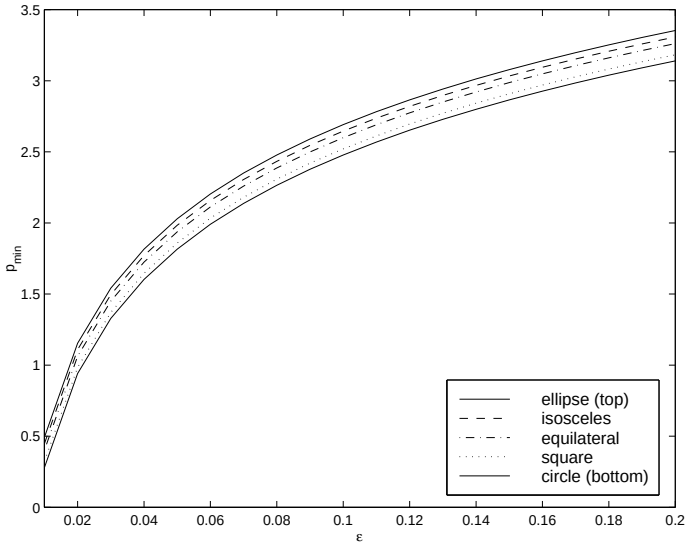

Figure 8: *Minimum oxygen partial pressure p_{min} versus ε, a measure of the capillary cross-sectional size, for various capillary shapes that all enclose an area of $\pi\varepsilon^2$, of one capillary concentric with a rectangular tissue domain with $-2 \le x_1 \le 2$ and $-1.5 \le x_2 \le 1.5$. Parameter values: $p_c = 5$, $\mathcal{M} = 0.5$, $\kappa = \infty$, $\mathcal{P} = 1$.*

6 Extensions

We remark on some possible extensions of our model.

Oxygen consumption rate $\mathcal{M} = \mathcal{M}(p)$. One way to extend this work is to consider an oxygen consumption rate that depends on the pressure, $\mathcal{M} = \mathcal{M}(p)$, where $d\mathcal{M}/dp > 0$. For instance, we consider the case of first-order kinetics for which $\mathcal{M}(p) = cp$ for some constant $c > 0$. For this special case, we would expand the asymptotic solution in the global region as in (4.5). The local problems in the region near each capillary, the specifications of the constants A_i, as well as the determination of the shape-parameters d_i, would remain the same as in the case of zero-order kinetics. We would then be able to determine a linear system for the A_i of the form (4.10c) where G and its regular part R are obtained from the Green's function of the reduced wave operator. For non-linear kinetics, such as Michaelis-Menten kinetics, the local analysis near each capillary remains the same, but the superposition principle leading to (4.10c) is no longer valid. For this case, there would be a non-linear capillary interaction.

Axial diffusion. We briefly discuss an extension to our work that considers axial diffusion in the tissue surrounding a capillary. Salathé et al. [17] used perturbation techniques in their study of axial diffusion in a Krogh cylinder geometry, whereas we propose to examine a capillary with a slowly-varying cross-section. For simplicity, we consider a tissue cylinder of radius 1 enclosing a single concentric capillary whose cross-sectional shape depends only on the axial variable, z. The governing equation for the oxygen partial pressure $p(r, z; \mu, \varepsilon)$ in the tissue is

$$\frac{\partial^2 p}{\partial r^2} + \frac{1}{r}\frac{\partial p}{\partial r} + \mu^2 \frac{\partial^2 p}{\partial z^2} = \mathcal{M}, \qquad \varepsilon f(z) < r < 1, \ 0 \le z \le L. \tag{6.1}$$

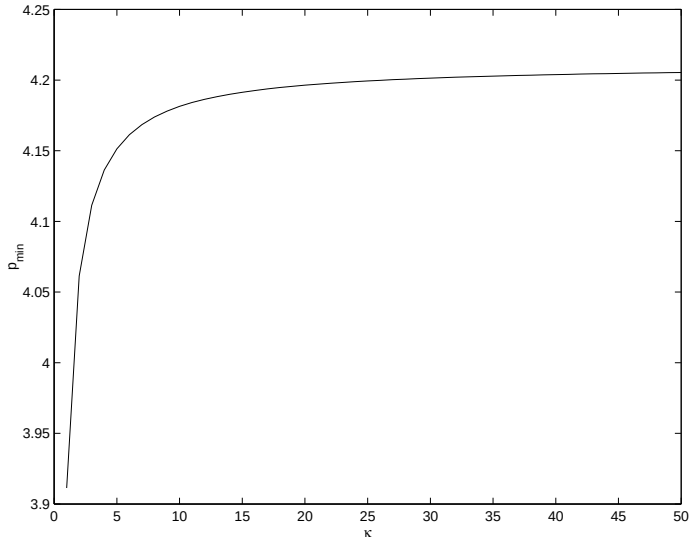

Figure 9: *Minimum oxygen partial pressure p_{min} versus κ for an elliptical tissue domain with semi-axes $a = 2$ and $b = 1$, containing one concentric, circular capillary of radius $\varepsilon = 0.1$. Parameter values: $p_c = 5$, $\mathcal{M} = 0.3$, $\mathcal{P} = 1$.*

Here, μ is a small parameter defined by

$$\mu^2 = \frac{\mathcal{P}_z^*}{\mathcal{P}_{\mathbf{x}}^*} \left(\frac{L_{\mathbf{x}}^*}{L_z^*} \right)^2 . \tag{6.2}$$

Typically, in skeletal muscle tissue, the intercapillary separation, $L_{\mathbf{x}}^*$, is a few microns whereas the capillary length, L_z^* is on the order of a thousand microns. As well, diffusivity in the axial direction, $\mathcal{P}_z^*$ is small relative to that in a transverse cut, $\mathcal{P}_{\mathbf{x}}^*$. The capillary has a radius of $\varepsilon f(z)$, where ε is a measure of the size of the capillary cross-section. For the analysis in §4 to be valid, we require that $\mu \ll (-1/\log \varepsilon)^a$, for any a.

The global region for the axial diffusion problem is the tissue volume away from the endpoints at $z = 0$ and $z = L$, in which we expand the solution as

$$p(r, z; \mu, \varepsilon) = p_0(r, z; \varepsilon) + \mu^2 p_1(r, z; \varepsilon) + \cdots , \tag{6.3}$$

provided that $\mu^2 \gg \varepsilon$. The function $p_0(r, z; \varepsilon)$ satisfies a slight variation of the two-dimensional oxygen transport problem. The global problems remain the same but, in the local region near the capillary, the shape-dependent parameter d is a function of the axial variable z.

Hence, if the axial diffusion is smaller than any power of $-1/\log \varepsilon$, the main result (4.10) still holds provided that we allow the shape-dependent parameters d_i to depend on the axial direction z. In addition, since in more physiologically realistic models, there can be a pressure gradient along the axis of the capillary, we could allow for the partial pressures p_{ci} at the capillary walls to depend on z. The decoupling of the global and local problems, inherent in (4.10), allows for an easy implementation of a more complicated physiological model inside each capillary.

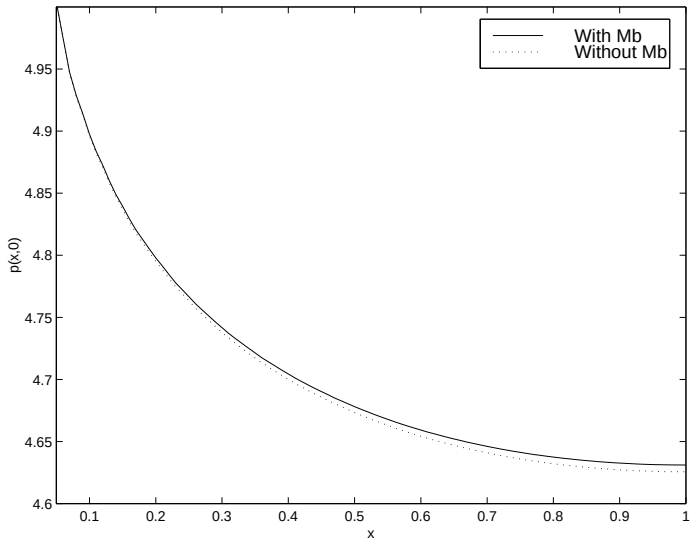

Figure 10: *Effect of myoglobin (Mb) facilitation on the oxygen partial pressure* $p(x,0)$ *versus radial position* x *in a circular tissue domain of radius 1 containing a concentric circular capillary of radius* $\varepsilon = 0.05$. *Parameter values:* $\mathcal{M} = 0.3$, $p_c = 5$, $p_F = 0.5$, $p_{0.5} = 1$, $\kappa = \infty$, $\mathcal{P} = 1$.

Acknowledgement

M.S.T. would like to thank Lorna Mornin of the Histology Laboratory at the University of British Columbia for the brief but informative tour of skeletal muscle tissue samples. We would like to thank the referees for their very helpful comments.

A Calculating the Modified Green's Function

For certain special cases, it is possible to solve (3.13) analytically for the modified Green's function. One such special case is that of a circular cross-section of tissue having radius a, with constant diffusivity $\mathcal{P} = \mathcal{P}_0$ in the tissue, and with a concentric capillary (singularity) located at the origin. In this case, the solution to (3.13) is

$$G(r) = \frac{1}{2\pi\mathcal{P}_0}\log r + \frac{1}{4\pi\mathcal{P}_0}\left(\frac{3}{2} - 2\log a - \frac{r^2}{a^2}\right). \tag{A.1}$$

For most other domains, we must solve (3.13) numerically to obtain $G(\mathbf{x};\boldsymbol{\zeta})$ and its regular part $R(\boldsymbol{\zeta})$. To do so, we used the *Partial Differential Equation Toolbox* [12], which is a finite element code of *Matlab*.

The numerical computation of G using the *PDE Toolbox* requires some care. To compute G numerically, we employ a regularization procedure by introducing a regularization parameter δ. We solve (3.13) for $G_\delta(\mathbf{x};\delta)$ with (3.13b) replaced by

$$\frac{\partial G_\delta}{\partial n} + \delta G_\delta = 0, \qquad \mathbf{x} \in \partial D. \tag{A.2}$$

This regularized problem has a unique solution for non-zero δ, where $\delta \ll 1$. We impose

the singularity structure from (3.13c) by decomposing G as

$$G_\delta(\mathbf{x};\boldsymbol{\zeta},\delta) = \frac{1}{2\pi\mathcal{P}(\boldsymbol{\zeta})}\log|\mathbf{x}-\boldsymbol{\zeta}| + R_\delta(\mathbf{x};\boldsymbol{\zeta},\delta). \tag{A.3}$$

Substituting (A.3) into (3.13), with (3.13b) replaced by (A.2), we obtain that $R_\delta(\mathbf{x};\boldsymbol{\zeta},\delta)$ is a regular function as $\mathbf{x}\to\boldsymbol{\zeta}$ that satisfies

$$\nabla\cdot[\mathcal{P}\nabla R_\delta] = -\frac{1}{A_D}, \qquad \mathbf{x}\in D, \tag{A.4a}$$

$$\frac{\partial R_\delta}{\partial n} + \delta R_\delta = \left[-\frac{1}{2\pi\mathcal{P}(\boldsymbol{\zeta})}\frac{\partial}{\partial n}\log|\mathbf{x}-\boldsymbol{\zeta}| - \frac{\delta}{2\pi\mathcal{P}(\boldsymbol{\zeta})}\log|\mathbf{x}-\boldsymbol{\zeta}|\right], \qquad \mathbf{x}\in\partial D, \tag{A.4b}$$

$$\int_D R_\delta(\mathbf{x};\boldsymbol{\zeta})\,d\mathbf{x} = -\frac{1}{2\pi\mathcal{P}(\boldsymbol{\zeta})}\int_D \log|\mathbf{x}-\boldsymbol{\zeta}|\,d\mathbf{x}. \tag{A.4c}$$

To compute the modified Green's function, we extrapolate the solution to (A.4) as $\delta\to 0$. One can show that the appropriate expansion of the solution to (A.4) as $\delta\to 0$ is $G_\delta(\mathbf{x};\boldsymbol{\zeta},\delta)\sim G_0(\mathbf{x};\boldsymbol{\zeta})+\delta G_1(\mathbf{x};\boldsymbol{\zeta})+\cdots$, and $R_\delta(\mathbf{x};\boldsymbol{\zeta},\delta)\sim R_0(\mathbf{x};\boldsymbol{\zeta})+\delta R_1(\mathbf{x};\boldsymbol{\zeta})+\cdots$, as $\delta\to 0$. We compute the regularized solution to (A.4a)–(A.4b) for two values of δ and call the resulting solutions $(R_{\delta_1})_c$ and $(R_{\delta_2})_c$. The size of δ we choose is bounded below by the tolerance δ_{cr} for our computed solution: e.g. $\delta>\delta_{cr}=0.001$. Then, we expand the computed solutions as $(R_{\delta_1})_c\sim R_{0c}+\delta_1 R_{1c}+\cdots$, and $(R_{\delta_2})_c\sim R_{0c}+\delta_2 R_{1c}+\cdots$. By a one-step extrapolation procedure, we obtain the solution $R_{0c}=[\delta_2(R_{\delta_1})_c-\delta_1(R_{\delta_2})_c]/(\delta_2-\delta_1)$. This solution is accurate up to terms of order $O(\delta^2)$. When $\delta=0$, the solution to (A.4a)–(A.4b) is not unique. To determine the additive constant, we substitute $R_\delta=R_{0c}+k$ into (A.4c) to obtain the constant k. Then, with an error of order $O(\delta^2)$, we have that

$$R(\mathbf{x};\boldsymbol{\zeta}) \sim R_{0c} - \frac{1}{A_D}\left[\frac{1}{2\pi\mathcal{P}(\boldsymbol{\zeta})}\int_D \log|\mathbf{x}-\boldsymbol{\zeta}|\,d\mathbf{x} + \int_D R_{0c}\,d\mathbf{x}\right]. \tag{A.5}$$

Finally, we use (A.5) in (A.3) as our numerical approximation for $G(\mathbf{x};\boldsymbol{\zeta})$.

Example: Krogh cylinder geometry. We test this computational technique on a special case for which we know the exact solution: a circular tissue domain of radius 1, with diffusivity $\mathcal{P}\equiv 1$ and containing a single concentric capillary. For this special case, the exact solution to (3.13) for the modified Green's function is the purely-radial solution in (A.1) with $a=1$ and $\mathcal{P}_0=1$. The regular part of the modified Green's function evaluated at the capillary location is

$$R(0) = \frac{3}{8\pi} \approx 0.1194. \tag{A.6}$$

We compare the regular part given in (A.6) for the exact solution with the numerical approximation for the regular part as we computed from our extrapolation procedure. We note that, since the singularity (capillary) is located at the origin and since the outer boundary is at $r=1$, the $\log|\mathbf{x}-\boldsymbol{\zeta}|$ term vanishes in (A.4b) and so the exact solution to the problem for the regular part is independent of δ. We test the dependence on δ of our computed solution $(R_\delta)_c$ for three pairs of δ_1 and δ_2. Table 4 contains the maximum absolute error, the $||L||_2$-norm of the error and the computed value of $R(0)$ for each of the δ-pairs, on a computational mesh containing 4,088 elements. The values in the table indicate that that the computed solution is essentially independent of δ.

$\{\delta_1, \delta_2\}$	$R_\delta(0)$	Maximum absolute error	$\|\|L\|\|_2$ of error
$\{0.025, 0.05\}$	0.1195	8.42e-04	0.0017
$\{0.01, 0.025\}$	0.1194	8.26e-04	0.0016
$\{0.01, 0.05\}$	0.1194	8.30e-04	0.0016

Table 4: *Test of δ-dependence on $R_\delta(0)$ using three pairs of δ values: maximum absolute error and L_2 norm of the error between $R_\delta(0)$ in* (A.5) *and the exact $R(0)$ in* (A.6).

B Determining a Unique Solution

The solution to (3.7) together with (3.10) is not unique. To address this point, we consider the corresponding eigenvalue problem for (ϕ_k, λ_k) which satisfies $\nabla \cdot [\mathcal{P}\nabla\phi_k] = -\lambda_k\phi_k$ in D, and $\partial\phi_k/\partial n = 0$ on ∂D. The first eigenpair for this problem is $(\phi_0, \lambda_0) = (1, 0)$, and the remaining eigenvalues, λ_k, are such that $0 < \lambda_1 \le \lambda_2 \le \ldots \le \lambda_k < \infty$.

We expand the solution $p^{(j)}(\mathbf{x})$, for $j \ge 1$, as a sum of the eigenfunctions

$$p^{(j)}(\mathbf{x}) = -\sum_{k=0}^{\infty} \frac{< b_j, \phi_k >}{\lambda_k < \phi_k, \phi_k >} \phi_k(\mathbf{x}). \tag{B.1}$$

Here, $b_j = e_{j1}\mathcal{M}(\mathbf{x}) + 2\pi \sum_{i=1}^{N} a_i^{(j)} \mathcal{P}(\boldsymbol{\xi}_i)\delta(\mathbf{x}-\boldsymbol{\xi}_i)$ is the right-hand side of (3.10) and $< f, g >$ is the inner product of the functions f and g defined by $< f, g >= \int_D f(\mathbf{x})g(\mathbf{x})\, d\mathbf{x}$. In (B.1), since $\lambda_0 = 0$, we require that $< b_j, \phi_0 >=< b_j, 1 >= 0$ for a solution to exist, and so the solvability condition for $p^{(j)}(\mathbf{x})$, for $j \ge 1$, is

$$\sum_{i=1}^{N} a_i^{(j)} \mathcal{P}(\boldsymbol{\xi}_i) = \begin{cases} -\dfrac{1}{2\pi} \displaystyle\int_D \mathcal{M}(\mathbf{x})\, d\mathbf{x}, & j = 1, \\ 0, & j \ge 2. \end{cases} \tag{B.2}$$

If (B.2) is satisfied, then we can write the solution $p^{(j)}(\mathbf{x})$, $j \ge 1$, as

$$p^{(j)}(\mathbf{x}) = -\sum_{k=1}^{\infty} \frac{< b_j, \phi_k >}{\lambda_k < \phi_k, \phi_k >} \phi_k(\mathbf{x}) + C_j\phi_0, \tag{B.3}$$

for any constant C_j. We need to fix the constant C_j in order to obtain a unique solution $p^{(j)}(\mathbf{x})$. Requiring that $< p^{(j)}, \phi_0 >= 0$, where $\phi_0 = 1$, is equivalent to $\int_D p^{(j)}(\mathbf{x})\, d\mathbf{x} = 0$. Using $< p^{(j)}, \phi_0 >= 0$ in (B.3) and applying the orthogonality condition of the eigenfunctions, we get that $C_j = 0$ for $j \ge 1$. Thus, we can decompose the solution $p^{(j)}(\mathbf{x})$ to (3.7) and (3.10), for $j \ge 1$, as $p^{(j)}(\mathbf{x}) = p_u^{(j)}(\mathbf{x}) + a_G^{(j)}$. In this decomposition, $a_G^{(j)}$ for $j \ge 1$ are global constants, and $p_u^{(j)}(\mathbf{x})$ is the unique solution to

$$\nabla \cdot [\mathcal{P}\nabla p_u^{(j)}] = e_{j1}\mathcal{M}(\mathbf{x}), \qquad \mathbf{x} \in D \setminus \bigcup_{i=1}^{N} \{\boldsymbol{\xi}_i\}, \tag{B.4a}$$

$$\frac{\partial p_u^{(j)}}{\partial n} = 0, \qquad \mathbf{x} \in \partial D, \tag{B.4b}$$

$$p_u^{(j)} \sim a_i^{(j)}(\log|\mathbf{x} - \boldsymbol{\xi}_i| + \mathcal{P}(\boldsymbol{\xi}_i)/\kappa_i) + a_i^{(j+1)} + e_{j1}p_{ci}, \qquad \mathbf{x} \to \boldsymbol{\xi}_i,\ i = 1, \ldots, N, \tag{B.4c}$$

$$\int_D p_u^{(j)}(\mathbf{x})\, d\mathbf{x} = 0. \tag{B.4d}$$

In (3.11), we used the further decomposition of $2\pi \sum_{i=1}^{N} a_i^{(j)} \mathcal{P}(\boldsymbol{\xi}_i) G(\mathbf{x}; \boldsymbol{\xi}_i) + e_{j1} p_R^{(1)}(\mathbf{x})$ instead of using $p_u^{(j)}(\mathbf{x})$.

References

[1] P. A. Clark, S. P. Kennedy, and A. Clark Jr. Buffering of muscle tissue PO_2 levels by the superposition of the oxygen field from many capillaries. In *Oxygen Transport to Tissue XI*, volume 248 of *Advances in Experimental Medicine and Biology*, pages 165–174. Plenum Press, New York and London, 1989.

[2] A. Dutta and A. S. Popel. A theoretical analysis of intracellular oxygen diffusion. *Journal of Theoretical Biology*, 176:433–445, 1995.

[3] M. L. Ellsworth, A. S. Popel, and R. N. Pittman. Assessment and impact of heterogeneities of convective oxygen transport parameters in capillaries of striated muscle: experimental and theoretical. *Microvascular Research*, 35:341–362, 1988.

[4] J. E. Fletcher. Mathematical modeling of the microcirculation. *Mathematical Biosciences*, 38:159–202, 1978.

[5] J. E. Fletcher. On facilitated oxygen diffusion in muscle tissues. *Biophysical Journal*, 29:437–458, 1980.

[6] P. R. Garabedian. *Partial Differential Equations*. John Wiley & Sons, Inc., New York, 1964.

[7] L. Hoofd. Updating the Krogh model – assumptions and extensions. In *Oxygen Transport in Biological Systems*, Society for Experimental Biology Seminar Series 51, pages 197–229. Cambridge University Press, Cambridge, 1992.

[8] L. Hoofd. Calculation of oxygen pressures in tissue with anisotropic capillary orientation. I. Two-dimensional analytical solution for arbitrary capillary characteristics. *Mathematical Biosciences*, 129:1–23, 1995.

[9] R. Hsu and T. W. Secomb. A Green's function method for analysis of oxygen delivery to tissue by microvascular networks. *Mathematical Biosciences*, 96:61–78, 1989.

[10] A. Krogh. The number and distribution of capillaries in muscles with calculations of the oxygen pressure head necessary for supplying the tissue. *Journal of Physiology (London)*, 52:409–415, 1919.

[11] M. C. Kropinski, M. J. Ward, and J. B. Keller. A hybrid asymptotic-numerical method for calculating low Reynolds number flows past symmetric cylindrical bodies. *SIAM Journal of Applied Mathematics*, 55:1484–1510, 1995.

[12] MathWorks, Inc. *Partial Differential Equations Toolbox, User's Guide*. MATLAB. The MathWorks, Inc., Natick, Mass., 1996.

[13] A. S. Popel. Analysis of capillary-tissue diffusion in multicapillary systems. *Mathematical Biosciences*, 39:187–211, 1978.

[14] A. S. Popel. Theory of oxygen transport to tissue. *Critical Reviews in Biomedical Engineering*, 17:257–321, 1989.

[15] T. Ransford. *Potential Theory in the Complex Plane*, volume 28 of *London Mathematical Society Student Texts*. Cambridge University Press, 1995.

[16] M. H. Ross, E. J. Reith, and L. J. Romrell. *Histology: A Text and Atlas*, chapter 10, page 204. Williams & Wilkins, Baltimore, Maryland, 2 edition, 1989.

[17] E. P. Salathé, T.-C. Wang, and J. F. Gross. Mathematical analysis of oxygen transport to tissue. *Mathematical Biosciences*, 51:89–115, 1980.

[18] R. C. Tai and H.-K. Chang. Oxygen transport in heterogeneous tissue. *Journal of Theoretical Biology*, 43:265–276, 1974.

[19] M. S. Titcombe and M. J. Ward. Convective heat transfer past small cylindrical bodies. *Studies in Applied Mathematics*, 91:81–105, 1997.

[20] M. J. Ward, W. D. Henshaw, and J. B. Keller. Summing logarithmic expansions for singularly perturbed eigenvalue problems. *SIAM Journal of Applied Mathematics*, 53(3):799–828, 1993.